ACS OMEGA

http://pubs.acs.org/journal/acsodf

Article

Preparation of Mn-Fe Oxide by a Hydrolysis-Driven Redox Method and Its Application in Formaldehyde Oxidation

Jie Ling, Yaxin Dong,* Pan Cao, Yixiang Wang, and YingYing Li

Cite This: *ACS Omega* 2021, 6, 23274−23280

Read Online

ACCESS | Metrics & More | Article Recommendations

ABSTRACT: Homogeneous distribution of Mn-Fe oxides (*x*Mn1Fe) with different Mn/Fe ratios was synthesized by a hydrolysis-driven redox method, and their catalytic activities in HCHO oxidation were investigated. The results showed that HCHO conversion was significantly improved after doping iron due to the synergistic effect between manganese and iron. The 5Mn1Fe catalyst exhibits excellent catalytic activity, achieving >90% HCHO conversion at 80 °C and nearly 100% conversion at 100 °C. The physicochemical properties of catalysts were characterized by BET, XRD, H_2-TPR, O_2-TPD, and XPS techniques. Experimental results revealed that the introduction of Fe into MnO_x resulted in a large surface area, a high ratio of Mn^{4+}, abundant lattice oxygen species and oxygen vacancy, and uniform distribution of Mn and Fe, thus facilitating the oxidation of HCHO to CO_2 and H_2O.

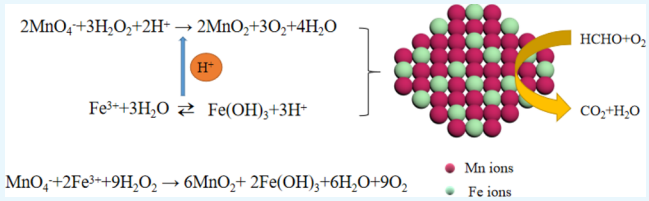

1. INTRODUCTION

The popularity of interior decoration has led to serious formaldehyde pollution. The average over-standard rate of formaldehyde in newly installed residential buildings is more than 70%, which is mainly derived from plywood, interior coatings, and furniture in decoration materials.[1] Formaldehyde can cause immunity decline, allergic dermatitis, and even poisoning, seriously endangering people's health.[2,3] Therefore, reducing and eliminating formaldehyde are of great significance for protecting the indoor air and human health.

The methods of eliminating formaldehyde in indoor air are mainly plant purification,[4] adsorption,[5] plasma purification,[6] photocatalysis,[7] and catalytic oxidation.[8] Catalytic oxidation is the most ideal method in eliminating formaldehyde compared to other physicochemical methods, which uses a catalyst to promote the reaction between formaldehyde and oxygen at low temperature to generate CO_2 and H_2O.[9] It has the advantages of high efficiency, easy control of operating conditions, minimal secondary pollution, and low energy consumption. The key factor of this method lies in the selection of effective catalysts to eliminate HCHO. Thus, improving the low-temperature oxidation activity of catalysts in formaldehyde purification is still evolving.

Among the catalysts for formaldehyde degradation, noble metal catalysts and transition metal oxide catalysts exhibit better performance and have been widely studied. However, a high-efficiency noble metal catalyst was limited in its large-scale application due to lack of resources and high cost. In contrast, a cost-effective and efficacious transition metal oxide catalyst could be used as a promising catalyst with abundant resources, low cost, and good redox properties.[10] Among them, manganese-based catalysts are excellent active components in various processes and are often used as catalysts or support materials.[11] The outer electron structure of manganese is $3d^5 4s^2$, and the convertible valence state can form oxides with different structures. Furthermore, the variable valence state of the manganese element in the manganese oxide will produce the internal defects and vacancies of the manganese oxide crystal, which is conducive to the movement and storage of oxygen. According to these literature studies, the preparation methods and synergistic effects among the active components play as key determinants of catalytic performance;[12] constructing a uniform distribution between varying metal oxide particles is the preparation target. The hydrolysis-driven redox method uses the coupling of two simultaneous reactions. In this method, $KMnO_4$ was reduced by H_2O_2 under acidic conditions, H^+ produced by Fe^{3+} hydrolysis can be used for Mn redox, and the consumed H^+ is beneficial to accelerate Fe^{3+} precipitation. At the same time, the conversion of H_2O_2 to H_2O and O_2 in the redox process is fully utilized. However, the conventional preparation methods such as impregnation and coprecipitation have disadvantages of easy agglomeration and difficult control of high dispersion of particles in mixed metal oxides. On the other hand, to improve the low-temperature

Received: June 8, 2021
Accepted: August 18, 2021
Published: September 1, 2021

oxidation activity of single metal oxides, metals, or metal oxides with a large atomic radius, weak M−O bond energy, and low electronegativity, elements such as Ce, Cu, Co, Fe, etc. are often added to manganese oxide to prepare a composite metal oxide catalyst. The Ce-MnO_2 catalyst prepared by Zhu *et al.* could completely convert HCHO at 100 °C and had better activity at low temperature than a single component.[13] Huang *et al.* reported that the $Co_xMn_{3-x}O_4$ nanosheets exhibited excellent catalytic activity that could convert HCHO to CO_2 at 100 °C.[14] In addition, Ma *et al.*[15] reported that iron oxides were the main active component to improve the catalytic activity of MnO_2-Fe_3O_4 in the catalytic combustion of toluene. Nevertheless, the application of MnO_2-Fe_3O_4 in catalytic oxidation of formaldehyde has not yet been widely studied.

In this work, we used the hydrolysis-driven redox reaction method to prepare uniform distribution of Mn-Fe oxides (*x*Mn1Fe) with different molar ratios of Mn/Fe. This method utilizes the coupling of two simultaneous reactions to synthesize Mn-Fe binary oxides. Also, the catalytic performances of those catalysts for formaldehyde oxidation were investigated. The relationship between the structure and catalytic performance of the catalysts was illustrated by the combination of BET, XRD, TPR, TPD, and XPS characterization techniques.

2. RESULTS AND DISCUSSION

2.1. Characterization of the Catalysts. *2.1.1. N_2 Adsorption and Desorption.* The N_2 adsorption−desorption isotherms of Mn-Fe oxides are illustrated in Figure 1, and the

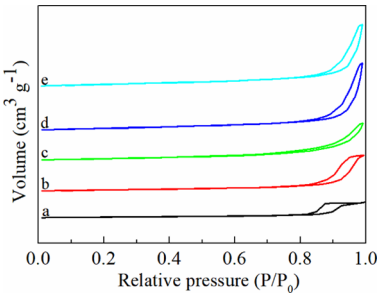

Figure 1. N_2 adsorption/desorption isotherm curves of (a) Fe_2O_3, (b) MnO_2, (c) 3Mn1Fe, (d) 5Mn1Fe, and (e) 7Mn1Fe.

Table 1. BET Surface Area, Pore Volume, and Pore Size of *x*Mn1Fe Catalysts Together with Fe_2O_3 and MnO_2

catalyst	S_{BET} (m^2 g^{-1})	pore diameter (nm)	pore volume (cm^3 g^{-1})
Fe_2O_3	54.3	13.9	0.3
MnO_2	103.1	18.2	0.5
3Mn1Fe	159.7	13.5	0.6
5Mn1Fe	184.5	21.2	1.1
7Mn1Fe	202.2	18.8	1.0

relative parameters are listed in Table 1. From Figure 1, it can be found that all the samples exhibited type III with H3 hysteresis, indicating the presence of a mesoporous structure. However, the isotherms of Fe_2O_3 are more similar to type V.[18] Different Mn/Fe molar ratios have significant effects on the microstructure of Mn-Fe oxides. The specific surface area of MnO_2 is 103.1 m^2 g^{-1}, which is much higher than that of Fe_2O_3 (54.3 m^2 g^{-1}). This result suggested that Fe_2O_3 samples prepared by the coprecipitation method have a lower S_{BET}. Also, the S_{BET} value can be further increased by introducing Fe ions; *x*Mn1Fe showed a similar value at 159.7−202.2 m^2 g^{-1}, which might be because the interaction between manganese and iron can effectively inhibit the structure growth of mixed oxides.[19] The values of pore diameter and pore volume for 5Mn1Fe were 21.2 nm and 1.1 cm^3 g^{-1}, respectively, which are larger than those of 3Mn1Fe and 7Mn1Fe. Overall, the larger pore volume and higher S_{BET} are beneficial to the catalytic oxidation. Therefore, 5Mn1Fe exhibited excellent catalytic performance.

2.1.2. XRD Patterns. The XRD measurement was performed to investigate the crystal structures of the MnO_2, Fe_2O_3, and *x*Mn1Fe samples. In Figure 2a, the Fe_2O_3 catalyst exhibits a

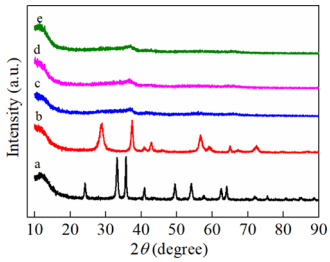

Figure 2. XRD patterns of (a) Fe_2O_3, (b) MnO_2, (c) 3Mn1Fe, (d) 5Mn1Fe, and (e) 7Mn1Fe.

typical pattern of α-Fe_2O_3 (JCPDS PDF 01-072-0469).[20] The primary peaks of MnO_2 appeared at 28.6, 37.4, and 56.8°, which is close to the pattern of α-MnO_2 (JCPDS PDF 44-0141).[21] Compared with MnO_2 samples, the incorporation of Fe led to a significant change in the diffraction pattern of *x*Mn1Fe catalysts. The intensity of the characteristic peak of MnO_2 decreases greatly or even disappears. This phenomenon indicates that the interaction between manganese and iron oxides makes the crystal form of MnO_2 change, showing an amorphous structure. According to the literature, poor crystallinity will lead to the loss of peaks and weakening of peak intensity.[22] In addition, only one characteristic diffraction peak of MnO_2 (37.1°) was observed in the three *x*Mn1Fe catalysts, and no characteristic peak of the Fe element was found, which indicated that Fe ions were highly dispersed on the surface of manganese oxide and did not form large grains, which provided evidence for the synthesis of homogeneous Mn-Fe binary oxides.

Meanwhile, the peak strength in the MnO_2 spectrum was decreased significantly with the increase in Fe content, indicating that the noncrystalline phase of MnO_2 was produced and Fe ions were highly dispersed on the manganese oxide surface. We can infer that the Fe ions in the MnO_2 lattice and the coexistence of manganese and iron oxides enhance this strong interaction, which are beneficial to produce more lattice defects and to increase the specific surface area of the samples.[23] It provides evidence for the synthesis of homogeneous Mn-Fe binary oxides.

2.1.3. H_2-TPR. The influence of different Mn/Fe ratios on *x*Mn1Fe binary oxide is also reflected in the difference of reduction ability. As shown in Figure 3, for the Fe_2O_3 sample, the reduction peak of Fe_2O_3 to Fe_3O_4 appeared at 361 °C and the other broad peaks were seen at 500−700 °C, corresponding to the reduction of Fe_3O_4 to FeO.[24] The

https://doi.org/10.1021/acsomega.1c02994
ACS Omega 2021, 6, 23274−23280

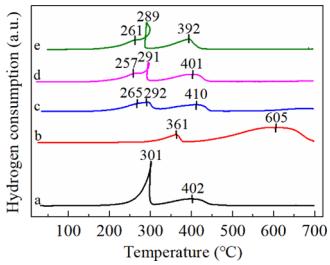

Figure 3. H_2-TPR profiles of (a) MnO_2, (b) Fe_2O_3, (c) 3Mn1Fe, (d) 5Mn1Fe, and (e) 7Mn1Fe.

MnO_2 pattern exhibited two obvious peaks at 301 and 402 °C, corresponding to the reduction of MnO_2 to Mn_2O_3 and Mn_2O_3 to MnO, respectively.[25] Compared to pure MnO_2 and *x*Mn1Fe samples, Fe doping significantly improves the reduction performance of the samples. Three reduction peaks appeared at about 260, 290, and 400 °C for 3Mn1Fe, 5Mn1Fe, and 7Mn1Fe, respectively. The first and third reduction peaks are attributed to the reduction process of $MnO_2 \rightarrow Mn_2O_3 \rightarrow MnO$, and the second peak is due to the reduction of Fe_2O_3 to Fe_3O_4. It can be seen that the reduction peaks of the three *x*Mn1Fe catalysts shift toward lower temperatures. This result reflects the strong interaction between Mn-Fe oxides, and Li *et al.*[38] also reached a similar conclusion in the study of NiMnFe mixed oxides.

In addition, the peaks of 5Mn1Fe and 7Mn1Fe overlapped with each other at 250−300 °C, which was caused by the instantaneous strong exothermic reaction between MnO_x and FeO_x. With the increase in manganese content to 7Mn1Fe, it can be found that the overlapping area of reduction peaks increases and the reduction peak area decreases. The low-temperature reducibility facilitates the enhancement of catalytic oxidation.[26,27] The order of reducibility increases as follows: 3Mn1Fe < 7Mn1Fe < 5Mn1Fe, which is in agreement with the activity test. High reducibility can encourage the mobility of oxygen species and promote the degradation of formaldehyde.[28]

2.1.4. O_2-TPD. O_2-TPD profiles of the catalysts were obtained to identify the mobility of the surface oxygen species. The physical adsorption of O_2 desorb at low temperature (<200 °C), and chemically adsorbed oxygen (O_2^- and O^-) desorbs between 200 and 400 °C, while the desorption peaks of lattice oxygen appear at high temperatures (>400 °C).[29] The desorption capacity of oxygen species obeys the following sequence: $O_2(ads) > O_2^-(ads) > O^-(ads) > O^{2-}(latt)$, where $O_2(ads)$ refers to physically adsorbed oxygen, $O_2^-(ads)$ means peroxy oxygen, $O^-(ads)$ represents monoatomic oxygen, and $O^{2-}(latt)$ indicates lattice oxygen.[30] As presented in Figure 4B, the Fe_2O_3 catalyst displayed that the desorption of chemical oxygen was dominant (200−500 °C) and had a low amount of $O^{2-}(latt)$ at a high temperature (637 °C). From Figure 4A, the MnO_2 and *x*Mn1Fe catalysts showed desorption peaks, which are attributed to the desorption of lattice oxygen. Especially for the 5Mn1Fe catalyst, the desorption peak appeared at 510 °C, which is lower than other *x*Mn1Fe catalysts. Meanwhile, it can be seen from Figure 4C that the desorption temperature of 5Mn1Fe is the lowest among the chemisorption oxygen peaks at 150−300 °C. It has been demonstrated that the desorption of surface active oxygen in 5Mn1Fe oxides is easier than those in pure MnO_2, 3Mn1Fe, and 7Mn1Fe, indicating the enhanced mobility of oxygen on its surfaces.[31]

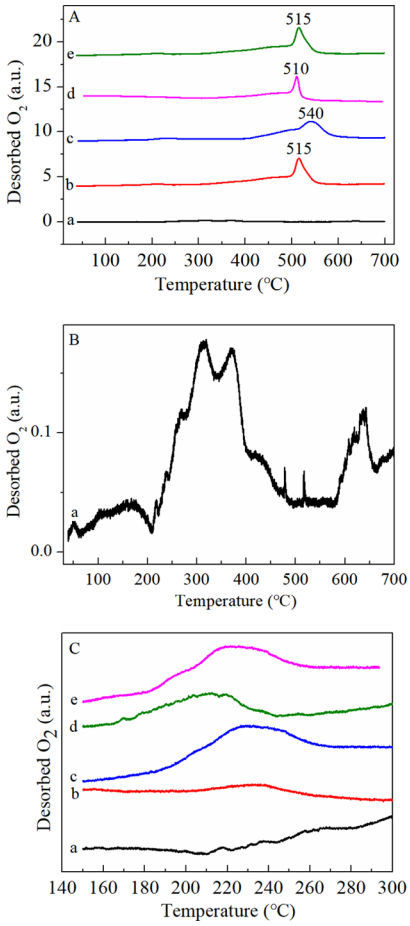

Figure 4. (A) O_2-TPD profiles of (a) Fe_2O_3, (b) MnO_2, (c) 3Mn1Fe, (d) 5Mn1Fe, and (e) 7Mn1Fe; (B) enlarged O_2-TPD profiles of (a) Fe_2O_3; and (C) enlarged O_2-TPD profiles at 150−300 °C.

2.1.5. XPS Characterization. The atomic concentration and chemical states of the surface elements (O, Mn, and Fe) over as-prepared samples were analyzed by XPS. Figure 5 displays

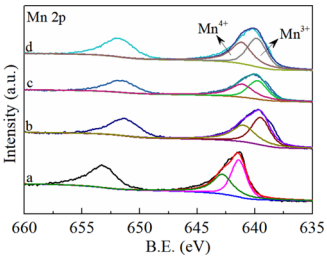

Figure 5. Mn 2p spectra of (a) MnO_2, (b) 3Mn1Fe, (c) 5Mn1Fe, and (d) 7Mn1Fe.

that the two peaks are discovered at 641.4 and 653.3 eV, which could be assigned to Mn-$2p_{3/2}$ and Mn-$2p_{1/2}$, respectively. Through the fitting analysis of the Mn$2p_{3/2}$ curve, the species of Mn^{3+} (639.6−641.3 eV) and Mn^{4+} (641.1−642.9 eV) can be detected.[32] Relative concentration ratios of Mn_x/Mn_{total} were calculated and are summarized in Table 2. The Mn^{4+}/Mn ratio in the MnO_2 sample was 43.8% lower than the Mn^{3+}/Mn ratio, indicating that the Mn species mainly exist in the form of Mn_2O_3. The introduction of Fe resulted in the increase in Mn^{4+} content, and the 5Mn1Fe catalyst exhibited a high value of 53.4%. This result may be due to the redox reaction between

https://doi.org/10.1021/acsomega.1c02994
ACS Omega 2021, 6, 23274−23280

Table 2. Surface Atomic Composite of the Catalysts Determined by XPS

	Mn_x/Mn_{total} (%)		O_x/O_{total} (%)		Fe_x/Fe_{total} (%)	
samples	Mn^{3+}	Mn^{4+}	O_β	O_α	Fe^{2+}	Fe^{3+}
Fe_2O_3			47.8	52.2	43.3	56.7
MnO_2	56.2	43.8	44.3	55.7		
3Mn1Fe	51.4	48.6	41.1	58.9	46.8	53.2
5Mn1Fe	46.6	53.4	37.2	62.8	57.1	42.9
7Mn1Fe	49.5	50.5	40.2	59.8	50.4	49.6

Mn and Fe oxides, leading to the transformation of Mn^{3+} to Mn^{4+}. As reported,[33] Mn^{4+} has the highest redox ability among all valence states of MnO_x, and a high ratio of Mn^{4+}/Mn is more favorable for the oxidation reaction.

Regarding the O 1s spectrum (Figure 6), two peaks featured at 527.7−529.0 and 529.2−531.3 eV correspond to lattice

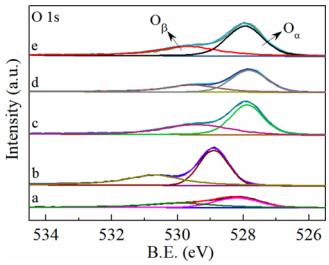

Figure 6. O 1s spectra of (a) Fe_2O_3, (b) MnO_2, (c) 3Mn1Fe, (d) 5Mn1Fe, and (e) 7Mn1Fe.

oxygen (named as O_α) and surface-absorbed oxygen (named as O_β), respectively.[34] Surface-adsorbed oxygen is mainly produced by gaseous oxygen adsorbed on oxygen vacancies on the catalyst surface, and lattice oxygen comes from surface oxygen in metal oxides. When lattice oxygen takes part in the reaction, an oxygen vacancy will be produced, thereby being immediately replenished by gaseous oxygen adsorption. From Table 2, the $O_\alpha/(O_\alpha + O_\beta)$ ratios are ranked as follows: Fe_2O_3 (52.2%) < MnO_2 (55.7%) < 3Mn1Fe (58.9%) < 7Mn1Fe (59.8%) < 5Mn1Fe (62.8%), suggesting that 5Mn1Fe possessed the most abundant lattice oxygen species, produced a large number of oxygen vacancies, and consumed the most gaseous oxygen. Therefore, it has the best catalytic effect.

The Fe-$2p_{3/2}$ spectra of the FMC catalyst are presented in Figure 7. One peak located at around 708.7 eV might be assigned to Fe^{2+} ions, and the other that appeared at 710.8 eV might be attributed to Fe^{3+} ions.[35] The contents of Fe^{2+} and

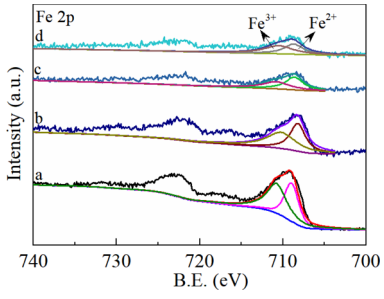

Figure 7. Fe 2p spectra of (a) Fe_2O_3, (b) 3Mn1Fe, (c) 5Mn1Fe, and (d) 7Mn1Fe.

Fe^{3+} in the samples are listed in Table 2. The Fe^{2+}/Fe ratio of 5Mn1Fe was 57.1% and obviously higher than those of 3Mn1Fe (46.8%) and 7Mn1Fe (50.4%); the increase in Fe^{2+} can be attributed to the redox equilibrium reaction between Mn and Fe. The redox pair between Mn^{4+}/Mn^{3+} and Fe^{3+}/Fe^{2+} may enhance the redox cycle, thereby promoting the generation of more oxygen vacancies and ultimately facilitating the catalytic oxidation reaction.[36,37]

2.2. Catalytic Activity. The catalytic activities of *x*Mn1Fe catalysts with varying ratios evaluated for HCHO conversion are shown in Figure 8. With the increase in reaction

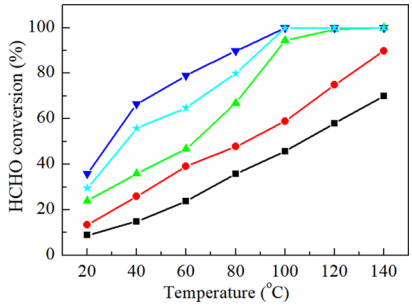

Figure 8. HCHO conversion over Fe_2O_3 (squares), MnO_2 (circles), 3Mn1Fe (triangles), 5Mn1Fe (inverted triangles), and 7Mn1Fe (stars). Reaction conditions: 250 ppm HCHO and 21 vol % O_2 and N_2 (balance). The total flow rate and weight hourly space velocity (WHSV) are 30 mL min^{-1} and 36,000 mL g_{cat}^{-1} h^{-1}, respectively.

temperature, HCHO conversion increased for all catalysts. Also, the different contents of the Mn-Fe mixed oxide catalyst have a great influence on the catalytic activity of HCHO oxidation. The HCHO conversion of pure Fe_2O_3 and MnO_2 was very low in the test range, and the conversion values are 69.4 and 90.2% at 140 °C, respectively. Compared with a single oxide catalyst, the catalytic activity of the *x*Mn1Fe mixed oxide catalyst was obviously higher. It is speculated that the high catalytic activity may be due to the interaction between MnO_x and FeO_y. Among all the catalysts, 5Mn1Fe exhibited the highest activity in HCHO conversion, achieving >90% HCHO conversion at 80 °C and nearly 100% conversion at 100 °C. In comparison, the MnO_2 catalyst exhibited only 49.1% conversion at 80 °C. The sequence of the catalytic activity of various catalysts is as follows: Fe_2O_3 < MnO_2 < 3Mn1Fe < 7Mn1Fe < 5Mn1Fe, which indicates the positive synergistic effect between Mn and Fe oxide. Meanwhile, manganese and iron oxide with a proper molar ratio could exhibit better catalytic activity, while an excessive amount of manganese has a negative influence. It is generally recognized that the metal state, structure and morphology, and redox properties are the main factors affecting the catalytic activity of the catalyst.[38] According to the XRD results, the introduction of Fe not only disperses iron itself but also boosts the dispersion of manganese oxide; therefore, Mn-Fe binary oxide has a higher surface area and thus is advantageous to adsorb more reactants to participate in the oxidation reaction. Combining the XPS results indicated that the introduction of Fe increased the concentration of surface Mn^{4+} and lattice oxygen species, increased the amount of oxygen vacancies and lattice defects, and also contributed to the HCHO catalytic oxidation reaction. Therefore, it was concluded that there is better dispersion of Mn and Fe oxides, a high content of surface Mn^{4+}, and a large number of lattice oxygen species.

https://doi.org/10.1021/acsomega.1c02994
ACS Omega 2021, 6, 23274−23280

Moreover, the hydrolysis-driven method plays an important role in the synthesis of high-efficiency Mn-Fe binary oxides, which can lead to catalysts with homogeneous distribution of active components, a more exposed surface area, and lower crystallinity.

3. EXPERIMENTAL SECTION

3.1. Catalyst Preparation. MnO_2 was fabricated by a redox reaction in acid solution.[16] Typically, 13 mmol of $KMnO_4$, 9.6 mmol of 98 wt % H_2SO_4, and 100 mL of deionized water were dissolved with stirring, and then a certain amount of H_2O_2 aqueous solution was slowly added into the above mixture. The mixture was continuously stirred for 6 h and then collected and washed with deionized water. After that, the drying treatment of products was performed at 100 °C for 12 h and heat treatment for 2 h at 400 °C.

A series of *x*Mn1Fe (where *x* denotes the Mn/Fe molar ratio in Mn-Fe oxides) samples were prepared by the hydrolysis-driven redox reaction method, similar to the literature.[17] $KMnO_4$ (38.1 mmol) and $Fe(NO_3)\cdot 9H_2O$ (12.6 mmol) were added into 300 mL of distilled water and stirred until completely dissolved. The mixed solution was added dropwise to a water solution of 570.4 mmol of H_2O_2 with vigorous stirring. After stirring at a constant speed for 6 h, the precipitate was collected by suction filtration and washed with distilled water several times. Finally, the product was dried in a vacuum oven to remove excess solution and roasted in a muffle furnace for 2 h at 400 °C. The obtained catalyst was denoted as $3MnO_y$-$1FeO_x$ (3Mn1Fe). It should be noted that hydrolysis of 1 mol of $Fe(NO)_3$ can produce 3 mol of H^+ in 3Mn1Fe to meet the theoretical requirement of nitric acid. Therefore, it is necessary to have a desired amount of HNO_3 when preparing Mn-Fe mixed oxides with different molar ratios. According to the corresponding Mn/Fe molar ratio, the catalysts were labeled as $5MnO_y$-$1FeO_x$ (5Mn1Fe) and $7MnO_y$-$1FeO_x$ (7Mn1Fe).

The Fe_2O_3 catalyst was prepared using the coprecipitation method. In brief, 14.9 mmol of $Fe(NO_3)\cdot 9H_2O$ was dispersed in 300 mL of distilled water and then mixed with 300 mL of aqueous solution containing 44.6 mmol of $NH_3\cdot H_2O$ with stirring at 30 °C. After that, the collection and treatment of brown solid were the same as the procedure described above.

3.2. Characterization. The Brunauer–Emmett–Teller (BET) specific surface area test was carried out using a micromeritics apparatus (ASAP2020HD88) at 77 K liquid nitrogen temperature under a N_2 atmosphere. Before analysis, the sample was degassed for 4 h at 250 °C.

Temperature-programmed reduction of H_2 (H_2-TPR) and temperature-programmed desorption of O_2 (O_2-TPD) were performed on a GC1690 chemical adsorption instrument. Fifty milligrams of catalyst was required for each test. In the TPR experiment, the catalyst was pretreated in an O_2/N_2 flow (30 mL min^{-1}) at 300 °C for 1 h and then cooled to room temperature. A 10 vol % H_2/N_2 reducing gas with a flow rate of 60 mL/min was introduced, and the TPR range was from room temperature to 700 °C at a rate of 10 °C/min. In the TPD experiment, the sample was first purged with helium at 200 °C for 1 h to purify the catalyst surface. Subsequently, the catalyst was allowed to react with O_2 for 0.5 h at 70 °C, and then He was introduced for 0.5 h to remove the adsorbed physical O_2. The adsorption of O_2 was measured in a He atmosphere by increasing the temperature to 700 °C, and the O_2 consumption was recorded continuously.

X-ray diffraction (XRD) patterns were obtained on a Bruker D8 Advance with Cu Kα radiation and a scanning diffraction angle (2θ) range of 10–80° with a scan step size of 5 °C min^{-1}.

X-ray photoelectron spectroscopy (XPS) measurement on a Thermo Scientific K-Alpha instrument used the C 1s peak position at 284.6 eV as the reference to calibrate the energy position of each peak.

3.3. Catalytic Activity Test. The catalyst (500 mg) with a size of 40–60 mesh was packed in a fixed-bed reactor with an inner diameter of 6 mm for the catalytic degradation of formaldehyde. Gaseous HCHO was produced by a flow of 21% O_2/N_2 over paraformaldehyde at 30 °C. The reaction feed contained 200 ppm HCHO and 21% O_2 and N_2 (constitute a balance). The total gas flow rate was maintained at 30 mL min^{-1}, and the corresponding mass space velocity (GHSV) was 36,000 mL g_{cat}^{-1} h^{-1}. The products (such as CO and CO_2) were analyzed by gas chromatography equipped with a thermal conductivity detector (TCD), hydrogen flame ionization detector (FID), and Ni catalyst converter. In the activity test, no other carbon compounds were detected in the catalyst products except CO_2. Thus, HCHO conversion is equal to the yield of CO_2 and calculated as follows:

$$\text{HCHO conversion (\%)} = \frac{[CO_2]_{out}}{[HCHO]_{in}} \times 100\%$$

where $[CO_2]_{out}$ is the outlet CO_2 concentration and $[HCHO]_{in}$ is the inlet HCHO concentration.

4. CONCLUSIONS

Homogeneous distribution of Mn-Fe oxides (*x*Mn1Fe) with different Mn/Fe ratios was developed by a hydrolysis-driven redox method. Among all the analyzed catalysts, the 5Mn1Fe catalyst exhibited superior catalytic activity for HCHO oxidation, achieving >90% HCHO conversion at 80 °C and nearly 100% conversion at 100 °C, results that reflect the positive synergistic effect between Mn and Fe oxide. According to the characterization results, it turns out that the enhanced catalytic activity can be ascribed to a high BET value, a large amount of Mn^{4+}, abundant lattice oxygen and oxygen vacancy, and uniform distribution of Mn and Fe. Overall, the introduction of Fe improves the catalytic activity of Mn-Fe binary oxides for HCHO oxidation.

AUTHOR INFORMATION

Corresponding Author

Yaxin Dong – *College of Chemistry and Chemical Engineering, Xi'an Shiyou University, Xi'an 710065, China*; orcid.org/0000-0002-7373-2638; Email: dong_yaxinn@163.com

Authors

Jie Ling – *College of Coal and Chemical Industry, Shaanxi Energy Institute, Hsienyang 712000, China*

Pan Cao – *College of Chemistry and Chemical Engineering, Xi'an Shiyou University, Xi'an 710065, China*

Yixiang Wang – *College of Chemistry and Chemical Engineering, Xi'an Shiyou University, Xi'an 710065, China*

YingYing Li – *College of Chemistry and Chemical Engineering, Xi'an Shiyou University, Xi'an 710065, China*

Complete contact information is available at: https://pubs.acs.org/10.1021/acsomega.1c02994

https://doi.org/10.1021/acsomega.1c02994
ACS Omega 2021, 6, 23274–23280

Notes

The authors declare no competing financial interest.

■ ACKNOWLEDGMENTS

This work was funded by the Youth Project of Shaanxi Science and Technology Department (2021JQ-886), the Natural Science Foundation of Shaanxi Education Department (19JK0194), and the National Natural Science Foundation of China (51074122). Meanwhile, the modern analysis and testing center of Xi'an Shiyou University provided strong support.

■ REFERENCES

(1) Bai, B. Y.; Qi, Q.; Li, J. H.; Hao, J. M. Progress in research on catalysts for catalytic oxidation of formaldehyde. *Chin. J. Catal.* **2016**, *37*, 102−122.
(2) Oliver, W. Vapochromism in organometallic and coordination complexes: chemical sensors for volatile organic compounds. *Chem. Rev.* **2013**, *113*, 3686−3733.
(3) Hakim, M.; Broza, Y. Y.; Barash, O.; Peled, N.; Phillips, M.; Amann, A.; Haick, H. Volatile Organic Compounds of Lung Cancer and Possible Biochemical Pathways. *Chem. Rev.* **2012**, *112*, 5945−5966.
(4) Kobayashi, T.; Shiratake, K.; Tabuchi, T. Studies for absorption of formaldehyde by using foliage on wild tomato species. *Hortic. J.* **2018**, *87*, 214−221.
(5) Chen, D.; Qu, Z.; Sun, Y.; Wang, Y. Adsorption-desorption behavior of gaseous formaldehyde on different porous Al_2O_3 materials. *Colloids Surf., A* **2014**, *441*, 433−440.
(6) Liang, W. J.; Li, J.; Li, J. X.; Zhu, T.; Jin, Y. Q. Formaldehyde removal from gas streams by means of $NaNO_2$ dielectric barrier discharge plasma. *J. Hazard. Mater.* **2010**, *175*, 1090−1095.
(7) Yu, J.; Wang, S.; Low, J.; Xiao, W. Enhanced photocatalytic performance of direct Z-scheme g-C_3N_4−TiO_2 photocatalysts for the decomposition of formaldehyde in air. *Phys. Chem. Chem. Phys.* **2013**, *15*, 16883−16890.
(8) Nie, L.; Yu, J.; Jaroniec, M.; Tao, F. Room-temperature catalytic oxidation of formaldehde on catalysts. *Catal. Sci. Technol.* **2016**, *6*, 3649−3669.
(9) Chen, J.; Yan, D. X.; Xu, Z.; Chen, X.; Xu, W.; Jia, H.; Che, J. A novel redox precipitation to synthesize Au-doped α-MnO_2 with high dispersion toward low Temperature oxidation of formaldehyde. *Environ. Sci. Technol.* **2018**, *52*, 4728−4737.
(10) Lu, S. H.; Wang, F.; Chen, C. C.; Huang, F. L. Catalytic oxidation of formaldehyde over CeO_2-Co_3O_4catalysts. *J. Rare Earths* **2017**, *35*, 867−874.
(11) Wang, C.; Chen, T.; Liu, H.; Xie, J.; Li, M.; Han, Z.; Zhao, Y.; He, H.; Zou, X.; Suib, S. L. Promotional catalytic oxidation of airborne Formaldehyde over mineralsupported MnO_2 at ambient temperature. *Appl. Clay Sci.* **2019**, *182*, 105289.
(12) Lu, S.; Chen, C.; Wang, X.; Wei, S.; Zhu, Q.; Huang, F.; Li, K.; Zhou, X.; He, L.; Liu, Y.; Pang, F. Efficient Catalytic Removal of Formaldehyde over Ag/Co_3O_4−CeO_2 Prepared by Different Method. *Catal. Surv. Asia* **2018**, *22*, 63−71.
(13) Zhu, L.; Wang, J.; Rong, S.; Wang, H.; Zhang, P. Cerium modified birnessite-type MnO_2 for gaseous formaldehyde oxidation at low temperature. *Appl. Catal., B* **2017**, *211*, 212−221.
(14) Huang, Y.; Ye, K.; Li, H.; Fan, W.; Zhao, F.; Yang, M. A highly durable catalyst based on $Co_xMn_{3-x}O_4$ nanosheets for low-temperature formaldehyde oxidation. *Nano Res.* **2016**, *9*, 3881−3892.
(15) Ma, W. J.; Huang, Q.; Xu, Y.; Chen, Y. W.; Zhu, S. M.; Shen, S. B. Catalytic combustion of toluene over Fe−Mn mixed oxides supported on cordierite. *Ceram. Int.* **2013**, *39*, 277−281.
(16) Chen, J.; Chen, X.; Xu, Z.; Xu, W. J.; Li, J. J.; Jia, H. P.; Chen, J. Syntheses of hierarchical MnO_2 via H_2O_2 selectively reducing $KMnO_4$ for catalytic combustion of toluene. *ChemistrySelect* **2016**, *1*, 4052−4056.
(17) Chen, J.; Chen, X.; Xu, W. J.; Xu, Z.; Chen, J.; Jia, H.; Chen, J. Hydrolysis driving redox reaction to synthesize Mn-Fe binary oxides as highly active catalysts for the removal of toluene. *Chem. Eng. J.* **2017**, *330*, 281−293.
(18) Kruk, M.; Jaroniec, M. Gas adsorption characterization of ordered organic-inorganic nanocomposite materials. *Chem. Mater.* **2001**, *13*, 3169−3183.
(19) Du, X. Y.; Li, C. T.; Zhao, L. K.; Zhang, J.; Lei, G.; Sheng, J.; Yi, Y.; Chen, J.; Zeng, G. Promotional removal of HCHO from simulated flue gas over Mn-Fe oxides modified activated coke. *Appl. Catal., B* **2018**, *232*, 37−48.
(20) An, N.; Wu, P.; Li, S.; Jia, M.; Zhang, W. Catalytic oxidation of formaldehyde over Pt/Fe_2O_3, catalysts prepared by different method. *Appl. Surf. Sci.* **2013**, *285*, 805−809.
(21) Lu, S.; Wang, X.; Zhu, Q.; Chen, C.; Zhou, X.; Huang, F.; Li, K.; He, L.; Liu, Y.; Pang, F. Ag−K/MnO_2 nanorods as highly efficient catalysts for form–aldehyde oxidation at low temperature. *RSC Adv.* **2018**, *8*, 14221−14228.
(22) Liu, F.; He, H.; Zhang, C.; Feng, Z.; Zheng, L.; Xie, Y.; Hu, T. Selective catalytic reduction of NO with NH_3 over iron titanate catalyst: Catalytic performance and characterization. *Appl. Catal., B* **2010**, *96*, 408−420.
(23) Sun, H.; Yu, X.; Ma, X.; Yang, X.; Lin, M.; Ge, M. MnO_x-CeO_2 catalyst derived from metal-organic frameworks for toluene oxidation. *Catal. Today* **2020**, *355*, 580−586.
(24) Chen, B. B.; Zhu, X. B.; Crocker, M.; Wang, Y.; Shi, C. FeO_x-supported gold catalysts for catalytic removal of formaldehyde at room temperature. *Appl. Catal., B* **2014**, *154*, 73−81.
(25) Huang, F.; Wang, X.; Zhu, Q.; Li, K.; Zhou, X.; Lu, S.; Fan, Z.; He, L.; Liu, Y.; Pang, F. Efficient Formaldehyde Elimination Over Ag/MnO_2 Nanorods: Influence of the Ag Loading. *Catal. Surv. Asia* **2019**, *23*, 33−40.
(26) Durán, F. G.; Barbero, B. P.; Cadús, L. E.; Rojas, C.; Centeno, M. A.; Odriozola, J. A. Manganese and iron oxides as combustion catalysts of volatile organic compounds. *Appl. Catal., B* **2009**, *92*, 194−201.
(27) Morales, M. R.; Barbero, B. P.; Cadús, L. E. Evaluation and characterization of Mn−Cu mixed oxide catalysts for ethanol total oxidation: influence of copper content. *Fuel* **2008**, *87*, 1177−1186.
(28) Zhang, C.; Li, Y.; Wang, Y.; He, H. Sodium-promoted Pd/TiO_2 for catalytic oxidation of formaldehyde at ambient temperature. *Environ. Sci. Technol.* **2014**, *48*, 5816−5822.
(29) Si, W.; Wang, Y.; Zhao, S.; Hu, F.; Li, J. A facile method for in situ preparation of the MnO_2/$LaMnO_3$ catalyst for the removal of toluene. *Environ. Sci. Technol.* **2016**, *50*, 4572−4578.
(30) Chen, X.; Yu, E.; Cai, S. C.; Jia, H. P.; Chen, J.; Liang, P. In situ pyrolysis of Ce-MOF to prepare CeO_2 catalyst with obviously improved catalytic performance for toluene combustion. *Chem. Eng. J.* **2018**, *344*, 469−479.
(31) Wang, M.; Zhang, L.; Huang, W.; Zhou, Y.; Zhao, H.; Lv, J.; Tian, J.; Kan, X.; Shi, J. Pt/MnO_2 nanosheets: facile synthesis and highly efficient catalyst for ethylene oxidation at low temperature. *RSC Adv.* **2017**, *7*, 14809−14815.
(32) Tang, Q.; Du, J.; Xie, B.; Yang, Y.; Yu, W.; Tao, C. Rare earth metal modified three dimensionally ordered macroporrous MnO_x-CeO_2 catalyst for diesel soot combustion. *J. Rare Earths* **2018**, *36*, 64−71.
(33) Shi, F.; Wang, F.; Dai, H.; Dai, J.; Deng, J.; Liu, Y.; Bai, G.; Ji, K.; Au, C. Rod-, flower-, and dumbbell-like MnO_2:Highly active catalysts for the combustion of toluene. *Appl. Catal., A* **2012**, *433-434*, 206−213.
(34) Zhang, J.; Li, Y.; Wang, L.; Zhang, C.; He, H. Catalytic oxidation of formaldehyde over manganese oxides with different crystal structures. *Catal. Sci. Technol.* **2015**, *5*, 2305−2313.
(35) Wang, T.; Wan, Z.; Yang, X.; Zhang, X.; Niu, X.; Sun, B. Promotional effect of iron modification on the catalytic properties of Mn-Fe/ ZSM-5 catalysts in the Fast SCR reaction. *Fuel Process. Technol.* **2018**, *169*, 112−121.

https://doi.org/10.1021/acsomega.1c02994
ACS Omega 2021, 6, 23274−23280

(36) Zhang, Y.; Zheng, Y.; Wang, X.; Lu, X. Preparation of Mn–FeO_x/CNTs catalysts by redox co-precipitation and application in low-temperature NO reduction with NH_3. *Catal. Commun.* **2015**, *62*, 57–61.
(37) Xiao, Y.; Huo, W.; Yin, S.; Jiang, D.; Zhang, Y.; Zhang, Z.; Liu, X.; Dong, F.; Wang, J.; Li, G.; Hu, X.; Yuan, X.; Yao, H.-C. One-step hydrothermal synthesis of Cu-doped MnO_2 coated diatomite for degradation of methylene blue in Fenton-like system. *J. Colloid Interface Sci.* **2019**, *556*, 466–475.
(38) Li, H.; Zhang, D.; Maitarad, P.; Shi, L.; Gao, R.; Zhang, J.; Cao, W. In situ synthesis of 3D flower-like NiMnFe mixed oxides as monolith catalysts for selective catalytic reduction of NO with NH_3. *Chem. Commun.* **2012**, *48*, 10645.

https://doi.org/10.1021/acsomega.1c02994
ACS Omega 2021, 6, 23274–23280